Chemical Geology 284 (2011) 306–316

Contents lists available at ScienceDirect

Chemical Geology

journal homepage: www.elsevier.com/locate/chemgeo

Research paper

Do carbonate precipitates affect dissolution kinetics? 1: Basaltic glass

Gabrielle J. Stockmann [a,*], Domenik Wolff-Boenisch [a], Sigurður R. Gislason [a], Eric H. Oelkers [b]

[a] Institute of Earth Sciences, University of Iceland, Sturlugata 7, 101 Reykjavík, Iceland
[b] GET-Université de Toulouse-CNRS-IRD-OMP, 14 Avenue Edouard Belin, 31400 Toulouse, France

ARTICLE INFO

Article history:
Received 1 October 2010
Received in revised form 9 March 2011
Accepted 10 March 2011
Available online 17 March 2011

Editor: U. Brand

Keywords:
Glass dissolution rates
CO_2 storage
Carbonate coating
Carbonatization
Mineral-carbon sequestration
Mixed-flow reactors

ABSTRACT

Basaltic glass dissolution rates were measured in mixed-flow reactors at basic pH and at 25 °C and 70 °C in aqueous solutions supersaturated with respect to calcite for up to 140 days. Inlet solutions were comprised of $NaHCO_3 \pm CaCl_2$ with ionic strengths >0.03 mol kg^{-1}. Scanning Electron Microscope images show that significant $CaCO_3$ precipitated during these experiments. This precipitate grew on the basaltic glass in experiments performed in Ca-free inlet solutions, but nucleated and grew independently of the glass surfaces in experiments performed in Ca-bearing inlet solutions. In those experiments where $CaCO_3$ precipitated on the glass surface, it grew as discrete crystals; no pervasive $CaCO_3$ layers were observed. The lack of structural match between glass and calcium carbonate favors $CaCO_3$ nucleation and growth as discrete crystals. Measured basaltic glass dissolution rates based on either Si, Al, or Mg were both 1) independent of time during the experiments, and 2) equal to that of corresponding control experiments performed in $NaHCO_3$-free inlet solutions. Taken together, these observations show that basaltic glass dissolution rates are unaffected by the precipitation of secondary $CaCO_3$ precipitation. It seems therefore likely that carbonate precipitation will not slow basaltic glass dissolution during mineral sequestration efforts in basaltic rocks.

1. Introduction

This study has been designed to elucidate the effect of secondary mineral precipitation on the dissolution rate of primary phases. The dissolution rates of minerals and glasses are commonly believed to be proportional to their surface area in contact with reactive fluid (e.g. Pačes, 1983; Helgeson et al., 1984; Lasaga, 1984; Siegel and Pfannkuch, 1984; Gautier et al., 2001; Oelkers, 2001; Schott et al., 2009). It seems likely therefore, that the precipitation of secondary phases could alter significantly the dissolution rates of those primary phases on which they precipitate. To test this possibility, the dissolution rates of basaltic glass have been measured in aqueous solutions that were supersaturated with respect to calcite.

Numerous studies have been performed in an attempt to determine the effect of secondary mineral precipitation on the dissolution rates of primary minerals in natural systems. Several authors suggested that the presence of mineral coatings is in part responsible for an apparent difference in laboratory versus natural mineral weathering rates (e.g. Nugent et al., 1998; White and Brantley, 2003). In contrast, Lee et al. (2008) concluded such coatings would be insufficiently continuous to significantly affect feldspar dissolution rates. Slow feldspar weathering rates in natural aquifers have been attributed to the coupling of secondary mineral precipitation to the dissolution of primary silicates (e.g. Zhu, 2005; Zhu et al., 2006, 2010). Velbel (1993) emphasized that the molar volume ratio of product to reactant has to be >1 to provide the volume needed to completely passivate the reactant surface.

Similarly, numerous studies have focused on the effect of secondary mineral precipitation on dissolution rates in the laboratory; these studies commonly present conflicting observations. For example, Murakami et al. (1998) suggested that secondary mineral formation could increase anorthite dissolution rates. In contrast, Hodson (2003) determined that the presence of iron-rich coatings had little effect on anorthite dissolution rates. Giammar et al. (2005) concluded that secondary magnesite precipitated as discrete particles would not limit forsterite dissolution in their experiments. Daval et al. (2009a) observed that secondary calcite coatings have only minor effects on the dissolution rates of wollastonite at acidic conditions, but could be significant at neutral pH. Daval et al. (2009b) described the formation of a non-passivating pseudomorphic silica-rich rim around wollastonite crystals. Both Béarat et al. (2006) and Andreani et al. (2009) reported that silica-rich layer formation on dissolving olivine surfaces slowed carbonate formation, and eventually inhibited olivine dissolution. Park and Fan (2004) suggested that silica-layers inhibited serpentine dissolution. Numerous studies have observed the slowing of glass dissolution rates due to the formation of pervasive leached layers (e.g. Cailleteau et al., 2008; Verney-Carron et al., 2010). Cubillas et al. (2005) concluded that the degree to which secondary mineral precipitation affects the dissolution rates of primary minerals depends on the relative structure of the precipitating versus the dissolving

* Corresponding author. Tel.: +354 525 5248; fax: +354 562 9767.
E-mail address: gjs3@hi.is (G.J. Stockmann).

0009-2541/$ – see front matter © 2011 Elsevier B.V. All rights reserved.
doi:10.1016/j.chemgeo.2011.03.010

Table 1
Chemical composition of the basaltic glass as measured with X-ray Fluorescence spectrometry (XRF).

	Stapafell Mountain, Iceland [a]	Stapafell Mountain, Iceland [b]
	Weight%	Weight%
SiO_2	48.25	48.12
Al_2O_3	14.95	14.62
CaO	11.85	11.84
Fe_2O_3	12.25	1.11
FeO		9.82
K_2O	0.309	0.29
MgO	9.50	9.08
MnO	0.187	0.191
Na_2O	2.01	1.97
P_2O_5	0.207	0.195
TiO_2	1.63	1.564
Total	101.14	99.89

[a] Glass used in this study. Iron was measured after oxidation of all Fe(II) to Fe(III) and thus Fe_2O_3 represents total Fe.
[b] XRF analysis results of Stapafell basaltic glass published by Oelkers and Gislason (2001).

mineral. If the precipitating mineral has a similar structure to the dissolving mineral, the secondary mineral can form a thin impermeable layer through an epitaxial growth mechanism arresting the dissolution of the underlying mineral. The degree that epitaxial growth occurs on a surface may also be affected by the degree of supersaturation (Lasaga, 1998). Similarly, Putnis (2009) found that the replacement of one mineral by another is closely related to the mineral structure and the relative volumes of the phases involved.

This study is focused on the dissolution of basaltic glass coupled to calcium carbonate precipitation. This system has been selected because of its potential application to carbon storage as part of *in-situ* mineral sequestration efforts (e.g. McGrail et al., 2006; Marini, 2007; Matter et al., 2007; Goldberg et al., 2008; Oelkers and Schott, 2005; Oelkers and Cole, 2008; Oelkers et al., 2008; Schaef and McGrail, 2009; Schaef et al., 2009; Gislason et al., 2010; Schaef et al., 2010). Carbon mineralization in basalts involves dissolution of the host rock releasing divalent metal cations such as Ca^{2+}, Mg^{2+}, and Fe^{2+} to solution. These ions can react with dissolved CO_2 and precipitate as carbonate minerals. The rate-limiting step for this reaction is thought to be the release of divalent cations (c.f., Oelkers et al., 2008). As such, any process that can potentially slow the dissolution rates of the basalt, such as secondary carbonate precipitation, would be detrimental to carbon storage efforts.

Towards the improved understanding of the effect of secondary minerals on the dissolution rates of primary solids, long-term basaltic glass dissolution experiments were performed in aqueous solutions supersaturated with respect to calcite in mixed-flows reactors. The purpose of this paper is to report the results of this experimental study and to apply these results to assess the potential effect of secondary carbonate precipitation on carbon mineralization efforts.

2. Theoretical background

The standard state adopted in this study is that of unit activity of pure minerals and H_2O at any temperature and pressure. For aqueous species other than H_2O, the standard state is unit activity of species in a hypothetical 1 mol kg^{-1} solution referenced to infinite dilution at any temperature and pressure. All thermodynamic calculations reported in this study were performed using the PHREEQC 2.14 computer code (Parkhurst and Appelo, 1999) together with its phreeqc.dat database to which thermodynamic data have been added for magnesite, thomsonite, scolecite, mesolite, laumontite, heulandite, analcime, Ca-stilbite, Ca-mordenite, Ca-clinoptilolite, Fe-celadonite, antigorite, amorphous FeOOH, allophane, and imogolite taken from Gysi and Stefansson (submitted for publication) and dawsonite from Benezeth et al. (2007). The thermodynamic properties of hydrated leached basaltic glass with the composition, $SiAl_{0.365}O_2(OH)_{1.095}$, was also added to this phreeqc.dat database. The equilibrium constant (K) for the leached glass dissolution reaction given by:

$$SiAl_{0.365}O_2(OH)_{1.095} + 1.095H^+ + 0.905H_2O = 0.365Al^{3+} + H_4SiO_4 \quad (1)$$

was calculated from the stoichiometric sum of the equilibrium constants of amorphous SiO_2 and amorphous $Al(OH)_3$ hydrolysis reactions (Wolff-Boenisch et al., 2004a). log K for reaction (1) is 1.23 with a ΔH_r equal to −24.04 kJ/mol at 25 °C.

3. Materials and methods

The basaltic glass used in this study was collected from the same location on the Stapafell Mountain in SW Iceland as that studied by Oelkers and Gislason (2001) and Gislason and Oelkers (2003). The chemical composition of the glass (Table 1) was determined by X-ray fluorescence spectrometry (XRF) and can be expressed as: $Si_{1.000}$ $Al_{0.365}$ $Fe_{0.191}$ $Mn_{0.003}$ $Mg_{0.294}$ $Ca_{0.263}$ $Na_{0.081}$ $K_{0.008}$ $Ti_{0.025}$ $P_{0.004}$ $O_{3.405}$. Iron is listed as total Fe as no attempt at determining Fe^{2+} was undertaken. However, the Fe^{2+}/Fe^{3+}-ratio in Stapafell basaltic glass was measured by Oelkers and Gislason (2001), and they showed Fe to be predominantly Fe^{2+} (see Table 1).

The basaltic glass was crushed in plastic bags using a plastic hammer. After crushing, the material was sieved and the 45–125 μm size fraction obtained. Fine particles were removed from this glass fraction by first gravity settling and then by ultrasonically cleaning the glass powder with cycles of water and then acetone. Altogether five water cycles and five acetone cycles were performed and the ultra fine suspension discarded at the end of each cycle. The final glass powder was then dried overnight at 60 °C. Solids before and after each experimental series were analyzed by Scanning Electron Microscopy (SEM) using a LEO Supra 25 and a JEOL 6360 LV Scanning Electron Microscope. The solids were coated with gold prior to this analysis. Energy Dispersive X-ray Spectroscopy (EDX) was used together with SEM to identify primary and secondary minerals. Selected samples were analyzed by X-ray diffraction (XRD) using an INEL CPS 120 to confirm the identity of secondary minerals. Fig. 1a shows the resulting glass powder after sieving and cleaning to be fine-particle free with an even distribution of all particle sizes from 45 to 125 μm. The specific surface area of the cleaned powder was determined to 5878 cm^2/g by 3-point krypton adsorption using the BET method. The density of this glass, as reported by Wolff-Boenisch et al. (2006), is 3.05 g/cm^3. The geometric surface area of the basaltic glass used in this study, A_{geo}, calculated using equations reported by Wolff-Boenisch et al. (2004a) is 251 cm^2/g. Dividing the BET surface area by the geometric surface area yields a roughness factor of 23. Although the glass surface appears smooth, the difference between BET and geometric surface area likely stems from fine scale porosity and roughness as can be seen in large magnification SEM images (see Fig. 1b).

The mixed-flow reactor system used for all experiments is illustrated in Fig. 2. This reactor system is similar to those used in past dissolution rate studies (e.g., Wolff-Boenisch et al., 2004a,b; Cubillas et al., 2005; Pokrovsky et al., 2005; Chaïrat et al., 2007; Gautelier et al., 2007). All reactors, connectors, and tubing were thoroughly cleaned in a 0.1 M HCl bath for ~24 h and rinsed with Millipore™ water prior to each experiment. All outlet fluid sample bottles went through the same cleaning procedure prior to sampling to prevent contamination. Basaltic glass dissolution experiments were initiated by placing either 5 or 10 g of cleaned basaltic glass powder and the selected inlet solution into the 300 mL polyethylene mixed-flow reactors. These reactors were sealed and placed into a temperature controlled water bath. Temperature was kept constant during the experiment at either 25 or 70 °C. Teflon™ coated floating stir bars from Nalgene™ were placed on the bottom of the reactors and propelled at stirring rates

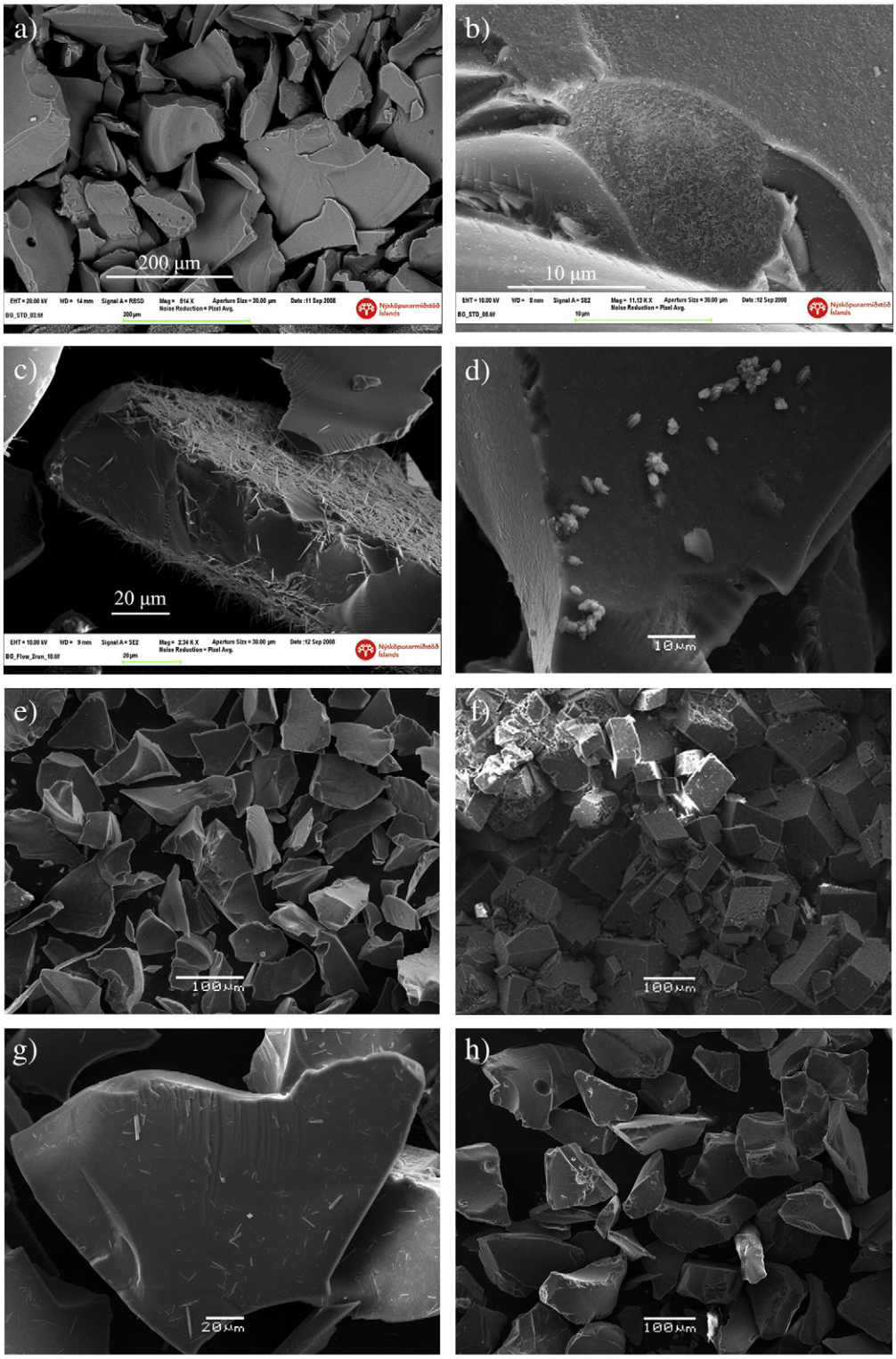

Fig. 1. Scanning electron images of the basaltic glass used in this study. Images a and b are of the basaltic glass before experiment. Image b is a magnification of image a showing surface roughness. Image c shows secondary silica-rich precipitates growing on the surfaces of glass following its dissolution during experimental series 2 at 70 °C, which is the only series, where other secondary phases than carbonates were observed. Image d depicts small $CaCO_3$ crystals growing out of the glass surface following its dissolution during series 8 at pH 10. Image e represents the surface of basaltic glass after dissolution during control series 9 at pH 10. Images f and g illustrate the morphology of $CaCO_3$ precipitates recovered from series 4 and 6. Calcite clusters as in f ranged in size from 10 to 1000 µm. Image h shows the surfaces of basaltic glass following its dissolution for ~164 days in control Exp. 7.

around 300 rpm using a multi-position magnetic stirrer located underneath the water bath. Floating stir bars were used to avoid grinding of the basaltic glass grains during the experiments.

Inlet solutions were comprised of Millipore™ water and Merck/Sigma-Aldrich analytical grade $NaHCO_3$, Na_2CO_3, NH_4Cl, $CaCl_2$, NaCl, NaOH, and/or HCl with ionic strengths ranging from 0.01 to 0.09 mol kg^{-1}. Compositions of the inlet solutions were based on calculations made using PHREEQC to yield the desired pH and ionic strength. The inlet solutions were stored in 8 or 12 L compressible plastic bags. Inlet solutions containing $CaCl_2$ were continuously

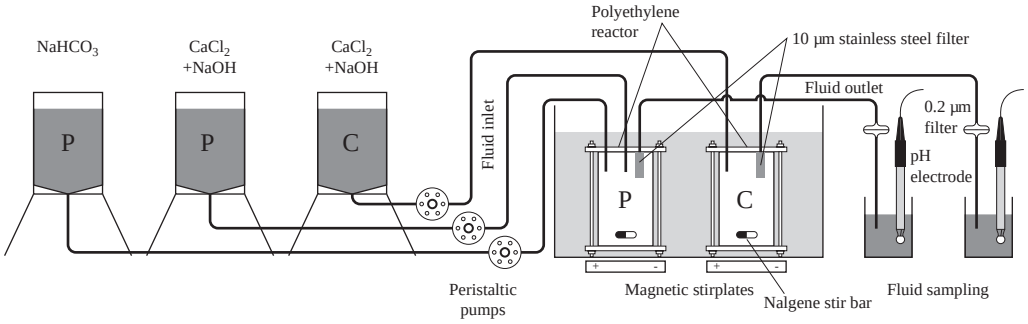

Fig. 2. Experimental setup of the precipitation (P) and control (C) experiments used for experimental series 4 through 7 at 25 °C. Supersaturation of calcite in the precipitation experiments is obtained by mixing two inlet solutions comprised of $NaHCO_3$ and $CaCl_2$, respectively, inside the reactor. The control experiments ran with a $CaCl_2$ inlet solution designed to dissolve basaltic glass without secondary precipitate formation. Both P and C reactors contained approximately 10 g of basaltic glass powder.

purged with N_2 to prevent atmospheric CO_2 from dissolving into this solution and to keep the pH stable. This effort was only partially successful as the pH in these solutions fluctuated ± 1 pH unit from the target pH. Inlet solutions were injected into the reactors at a constant rate using Masterflex™ cartridge pumps. In some experiments two inlet solutions (one Ca-rich and the second carbonate-rich) were used to create a solution supersaturated with respect to calcite in the reactor.

Experiments in this study were performed in series consisting of a sequence of runs performed on a single basaltic glass powder. For each experiment in a series the temperature and inlet solution flow rate were kept constant while the chemical composition of the inlet solution was changed. Two different types of experiments were performed: 'precipitation' and control 'experiments'. 'Precipitation' experiments were designed to measure basaltic glass dissolution rates during carbonate precipitation. To attain calcite saturation, carbonate ±calcium were provided to the system by the inlet solutions. 'Control' experiments were designed to measure basaltic glass dissolution rates in the absence of secondary phase precipitation and were carried out in carbonate-free inlet solutions. Details of all nine experimental series are provided in Tables 2–4. Each series is denoted by a number, and each experiment within a series is indicated by a letter, i.e. Exp. 7a–e are five experiments within series 7.

Outlet fluids were regularly sampled during all experiments. Three residence times or more separated each sampling. The residence time is defined as the volume of the reactor divided by the fluid flow rate. The outlet solutions were filtered through a 0.2 μm cellulose acetate membrane filter into a 100 mL polyethylene bottle and acidified with concentrated supra-pure HNO_3. The major element concentrations of inlet and outlet fluids were determined using a Spectro Ciros Vision Inductively Coupled Plasma Optical Emission Spectrometer (ICP-OES). Analytical uncertainties on ICP-OES analyses are estimated to be 3–5%.

Glass dissolution rates based on the release of the *i*th element ($r_{+,i,j}$) were calculated from:

$$r_{+,i,j} = \frac{C_i \cdot fr}{\nu_i \cdot A_j \cdot m} \quad (2)$$

where C_i stands for the concentration of the *i*th element in the outlet solution, *fr* refers to the fluid flow rate, ν_i is the stoichiometric factor of the *i*th element, A_j designates the specific surface area of the basaltic glass, and *m* denotes the mass of glass used in the experiment. The

Table 2
Composition of the inlet fluids for the all experiments performed in this study.

Experiment[a]	$NaHCO_3$ (mol/kg)	NH_4Cl (mol/kg)	$CaCl_2$ (mol/kg)	Na_2CO_3 (mol/kg)	NaCl (mol/kg)	NaOH (mol/kg)	HCl (mol/kg)[c]	Ionic strength (mol/kg)	pH (21 °C)
1a-P	0.035							0.035	8.45
1b-P	0.035						n.m.	0.035	6.35
2-P	0.035							0.035	8.54
3-C		0.010						0.010	5.74
4-P[b]	0.035		0.010					0.033	8.15
5a-C			0.014			1.0E−06		0.042	7.29
5b-C			0.020			1.4E−06		0.060	7.22
6a-P[b]	0.035		0.010			1.2E−07		0.033	n.m.
6b-P[b]	0.035		0.020			1.6E−07		0.048	n.m.
6c-P	0.010							0.010	8.54
6d-P		0.010					n.m.	0.010	3.81
7a-C			0.020			1.6E−07		0.060	7.92
7b-C			0.030			1.7E−07		0.090	8.33
7c-C			0.030					0.090	5.83
7d-C	0.010							0.010	8.54
7e-C		0.010					n.m.	0.010	3.81
8a-P	0.010			0.010				0.040	10.12
8b-P	0.010			0.010				0.040	10.13
8c-P	0.010							0.010	8.54
9a-C					0.035	1.3E−07		0.035	10.18
9b-C					0.035	1.3E−07		0.035	10.19
9c-C	0.010							0.010	8.54

n.m. = not measured.
[a] The '-P' and '-C' designates precipitation and control experiments, respectively.
[b] Two-inlet system, i.e. the concentration of the fluid entering the reactor is half of each inlet.
[c] HCl was added until the desired pH was reached, but the exact concentration was not measured.

index *j* refer to rates calculated either using the measured BET surface area, A_{BET} or the geometric surface area, A_{geo}.

Thermodynamic calculations suggest the some of the outlet fluids at both 25 and 70 °C were supersaturated with respect to several secondary phases including gibbsite, hematite, goethite, zeolites and clay minerals. These are minerals that occur naturally in the Hellisheidi basalts (Alfredsson et al., 2008). Secondary iron phases were supersaturated in most experiments and often a reddish-brown precipitate was observed on the stainless steel filters inside the mixed-flow reactors. Thermodynamic calculations also indicate that the outlet fluids were all strongly undersaturated with respect to the dissolving basaltic glass itself with a chemical affinity; $A^* \geq 10$ kJ/mol in all experiments, where A^* refers to the chemical affinity of the hydrated surface layer (c.f., Gislason and Oelkers, 2003).

4. Experimental results

In total, 19 steady-state dissolution experiments were performed as part of 9 experimental series. The chemical compositions of the inlet fluids, their pH and ionic strength are listed in Table 2. Compositions of the outlet fluids at steady-state and calculated steady-state basaltic glass dissolution rates for all 19 experiments are listed in Tables 3a and b. The saturation state of calcite in the outlet fluids and other selected minerals are provided in Table 4. These experimental results will be discussed in detail below.

4.1. Basaltic glass dissolution in aqueous carbonate inlet fluids at 70 °C (experimental series 1 and 2)

Experimental series 1 and 2 dissolved basaltic glass in 0.035 mol kg^{-1} $NaHCO_3$ inlet solutions. Experimental series 1 was previously described by Stockmann et al. (2008), a preliminary report of this study. Results for this experimental series in the current manuscript differ somewhat from those previously reported because they have been corrected for loss of dissolving basaltic glass mass during the experiment. The initial mass of 9.9 g of basaltic glass was reduced by dissolution to 8.8 g during the experiment, which makes a notable difference in calculated rates. Mass-corrected results of experimental series 1 are shown as a function

Table 3
Physical conditions, steady-state solution compositions, and measured basaltic glass dissolution rates of all experiments performed in the present study.

a. Physical conditions and steady-state fluid compositions of the basaltic glass dissolution experiments performed in this study.

Exp.[c]	T (°C)	m_{BG} (g)	S_{BET} (m^2)	*fr* (g/min)	t_{exp} (days)	pH_{out} in-situ T[a]	$[Si]_{out}$ (μmol/kg)	$[Al]_{out}$ (μmol/kg)	$[Ca]_{out}$ (μmol/kg)	$[Mg]_{out}$ (μmol/kg)	$[Fe]_{out}$ (μmol/kg)	A* (kJ/mol)[a]	log (a^2_{H+}/a_{Al3+})[a]
1a-P	70	9.93	5.84	0.56	42	8.2	244.82	78.47	19.47	62.04	0.15	13.4	−6.3
2-P	70	9.82	5.77	0.57	26	8.1	129.72	38.38	20.90	30.37	0.04	15.1	−6.1
3-C	70	5.00	2.94	1.17	10	5.2	19.71	0.10	3.31	2.86	0.26	21.7	−5.6
4-P	25	9.98	5.87	0.51	64	7.1	5.03	0.09	2370.25[b]	9.53[b]	0.05	20.2	−9.2
5a-C	25	9.92	5.83	0.51	12	6.8	5.86	0.33	n.m.[b]	22.90[b]	0.05	17.7	−9.2
5b-C	25	9.92	5.83	0.51	48	6.8	8.75	1.17	n.m.[b]	30.20[b]	0.03	16.0	[d]
6a-P	25	9.53	5.60	0.50	29	7.2	7.47	0.14	2517.38[b]	9.29[b]	0.10	18.5	−8.6
6b-P	25	9.53	5.60	0.50	40	7.0	4.26	0.23	5913.36[b]	15.79[b]	0.08	19.1	−8.9
6c-P	25	5.09	2.99	0.63	8	8.6	4.24	1.57	53.82	1.31	0.06	20.6	−8.3
6d-P	25	5.09	2.99	0.64	5	8.1	4.64	1.36	794.66	1.61	0.03	19.4	−8.7
7a-C	25	9.85	5.79	0.45	32	7.7	14.93	3.83	n.m.[b]	30.70[b]	0.08	14.9	[d]
7b-C	25	9.85	5.79	0.49	114	7.9	14.54	4.31	n.m.[b]	42.18[b]	0.04	15.5	[d]
7d-C	25	5.13	3.02	0.63	9	8.5	4.63	1.70	n.m.	1.12	0.29	20.3	−8.3
8a-P	25	9.75	5.73	0.48	146	10.0	14.86	2.76	4.66	3.60	b.d.	22.9	−7.0
8b-P	25	5.01	2.94	0.72	7	10.1	11.75	2.12	7.46	2.92	b.d.	23.7	−6.9
8c-P	25	5.01	2.94	0.72	5	8.6	5.15	1.21	7.09	2.33	0.12	20.5	−8.1
9a-C	25	9.41	5.53	0.47	132	9.9	11.79	3.54	n.m.	2.14	0.03	18.8	−7.2
9b-C	25	5.03	2.96	0.70	7	10.0	11.48	3.59	n.m.	1.96	0.16	22.6	−7.2
9c-C	25	5.03	2.96	0.69	5	8.5	4.11	0.83	n.m.	1.66	0.02	21.4	−8.0

b. Steady-state basaltic glass dissolution rates (log r_+) in mol/cm^2/s obtained in this study

Exp.	T (°C)	pH_{out} at in-situ T	log $r_{+,Si,BET}$	log $r_{+,Si,geo}$	log $r_{+,Al,BET}$	log $r_{+,Al,geo}$	log $r_{+,Ca,BET}$	log $r_{+,Ca,geo}$	log $r_{+,Mg,BET}$	log $r_{+,Mg,geo}$	log $r_{+,Fe,BET}$	log $r_{+,Fe,geo}$
1a-P	70	8.2	−13.4	−12.0	−13.5	−12.1	−13.9	−12.6	−13.5	−12.1	−15.9	−14.5
2-P	70	8.1	−13.7	−12.3	−13.8	−12.4	−13.9	−12.5	−13.8	−12.4	−16.5	−15.1
3-C	70	5.2	−13.9	−12.5	−15.7	−14.4	−14.1	−12.7	−14.2	−12.8	−15.0	−13.7
4-P	25	7.1	−15.1	−13.8	−16.4	−15.1					−16.4	−15.1
5a-C	25	6.8	−15.1	−13.7	−15.9	−14.5					−16.4	−15.0
5b-C	25	6.8	−14.9	−13.5	−15.3	−14.0					−16.6	−15.3
6a-P	25	7.2	−15.0	−13.6	−16.2	−14.9					−16.1	−14.7
6b-P	25	7.0	−15.2	−13.8	−16.0	−14.7					−16.2	−14.8
6c-P	25	8.6	−14.8	−13.5	−14.8	−13.5	−13.1	−11.8	−14.8	−13.4	−16.0	−14.6
6d-P	25	8.1	−14.8	−13.4	−14.9	−13.5	−12.0	−10.6	−14.7	−13.3	−16.3	−14.9
7a-C	25	7.7	−14.7	−13.3	−14.9	−13.5					−16.3	−14.9
7b-C	25	7.9	−14.7	−13.3	−14.8	−13.4					−16.5	−15.2
7d-C	25	8.5	−14.8	−13.4	−14.8	−13.4			−14.9	−13.5	−15.3	−13.9
8a-P	25	10.0	−14.7	−13.3	−15.0	−13.6	−14.6	−13.2	−14.8	−13.4		
8b-P	25	10.1	−14.3	−13.0	−14.6	−13.3	−13.9	−12.6	−14.4	−13.0		
8c-P	25	8.6	−14.7	−13.3	−14.9	−13.5	−14.0	−12.6	−14.5	−13.1	−15.6	−14.2
9a-C	25	9.9	−14.8	−13.4	−14.9	−13.5			−15.0	−13.6	−16.7	−15.3
9b-C	25	10.0	−14.3	−13.0	−14.4	−13.0			−14.6	−13.2	−15.5	−14.1
9c-C	25	8.5	−14.8	−13.4	−15.1	−13.7			−14.7	−13.3	−16.4	−15.0

n.m. = not measured. b.d. = below detection limit.
[a] Computed with PHREEQC version 2.14.
[b] Ca and Mg concentrations arise from $CaCl_2$ inlet solution.
[c] The '-P' and '-C' designates precipitation and control experiments, respectively.
[d] No stable value, not included.

Table 4
Saturation indices (SI) of selected minerals in the outlet fluids of all experiments reported in this study.[a,b,c]

Exp.[d]	Calcite	Aragonite	Gibbsite	Amorph. $Al(OH)_3$	Goethite	Hematite	Amorph. FeOOH[e]	Amorph. SiO_2	Chlorite	Kaolinite	Mesolite[e]	Scolecite[e]	Thomsonite[e]	Other minerals super-saturated according to modeling[a]
1a-P	−0.02	−0.14	0.37	−1.97	5.46	13.11	−0.09	−1.26	6.10	1.22	1.44	1.64	3.69	Allophane, analcime, chrysotile, dawsonite, dolomite, imogolite, Ca-mordenite, magnesite, talc
2-P	−0.05	−0.16	0.21	−2.13	5.23	12.66	−0.32	−1.51	2.18	0.40	0.16	0.38	1.15	Allophane, analcime, dawsonite, dolomite, imogolite, magnesite, talc
3-C			−0.35	−2.68	−4.10	−6.02	−9.66	−2.33	−33.50	−2.34	−10.66	−9.29	−21.82	
4-P	0.24	0.10	−0.10	−2.79	5.25	12.51	−0.65	−2.57	−23.34	−1.98	−5.58	−4.52	−10.44	
5a-C			1.10	−1.59	4.48	10.96	−1.43	−2.52	−22.25	0.52	−5.58	−1.87	−7.94	Allophane, imogolite
5b-C			1.52	−1.17	4.45	10.90	−1.46	−2.37	−20.13	1.66	−3.98	−0.41	−4.44	Allophane, imogolite
6a-P	0.45	0.30	0.59	−1.04	5.24	12.50	−0.65	−2.51	−22.03	−0.49	−3.97	−2.89	−6.55	Dawsonite, imogolite
6b-P	0.50	0.36	0.83	−0.80	4.96	11.92	−0.95	−2.68	−22.65	−0.34	−4.07	−2.90	−6.30	Dawsonite, imogolite
6c-P	0.10	−0.04	0.15	−2.54	6.10	14.21	0.20	−2.69	−13.09	−1.72	−3.76	−3.13	−6.04	
6d-P	−5.83	−5.97	0.57	−2.12	−1.29	−0.57	−7.19	−2.63	−16.30	−0.76	−4.57	−1.95	−6.23	
7a-C			1.28	−1.41	5.89	13.79	−0.01	−2.11	−10.91	1.70	−1.79	1.73	0.32	Allophane, imogolite
7b-C			1.14	−1.55	5.80	13.60	−0.11	−2.15	−9.07	1.35	−1.78	1.82	0.52	Allophane, imogolite
7d-C	−0.24	−0.39	0.17	−2.52	6.72	15.44	0.81	−2.67	−13.78	−1.65	−3.96	−3.43	−6.67	
8a-P	−0.06	−0.21	−1.19	−3.88				−2.63	−1.35	−4.28	−4.10	−4.29	−7.85	
8b-P	0.04	−0.11	−1.27	−3.96				−2.71	−1.69	−4.59	−4.37	−4.52	−8.29	
8c-P	−0.65	−0.79	−0.03	−2.72	6.49	14.99	0.59	−2.58	−10.67	−1.86	−4.13	−3.78	−7.51	
9a-C			−0.91	−3.60	4.96	11.92	−0.95	−2.62	−0.49	−3.70	−3.19	−3.21	−5.43	
9b-C			−0.95	−3.64	5.53	13.06	−0.38	−2.66	−0.46	−3.84	−3.02	−2.90	−4.77	
9c-C	−0.82	−0.97	−0.23	−2.92	5.56	13.13	−0.34	−2.80	−14.42	−2.68	−5.54	−5.20	−10.49	

[a] Computed with PHREEQC version 2.14.
[b] Saturation index is defined as: $SI = \log(IAP/K_{sp})$, where IAP is the ion activity product and K_{sp} refers to the solubility product of the solid phase.
[c] Uncertainty on SI is estimated to ±0.10 log units.
[d] The '-P' and '-C' designates precipitation and control experiments, respectively.
[e] Based on data from Gysi and Stefansson (submitted for publication).

of time in Fig. 3a. Basaltic glass dissolution rates based on Si, Al, and Mg release are similar and thus consistent with the stoichiometric dissolution of the glass during the first 42 days of the experiment. The pH of the outlet fluid was constant and equal to 8.2 during the experiment. The dissolution of the glass also released Ca to solution. The combination of this Ca release and the HCO_3^- present in the inlet solution resulted in the reactive fluid being saturated with respect to calcite (Fig. 3b). The dissolution rates based on Ca shown in Fig. 3a are 0.5 log units slower than that of the other elements, consistent with the precipitation of a calcium carbonate phase. Calculations indicate that the reactive fluids are also supersaturated with respect to gibbsite, goethite, hematite, dawsonite, dolomite, magnesite, chlorite, chrysotile, talc, kaolinite, allophane, imogolite and several zeolites. Dissolution rates based on Fe are not shown in Fig. 3a as their concentration in the outlet fluids are at or below the analytical detection limit suggesting Fe-oxyhydroxide precipitation. In contrast the relative dissolution rates based on Si, Al, and Mg are consistent with the absence of significant quantities of Mg or Al bearing secondary phases.

After 42 days, the original inlet solution was replaced by a 0.035 mol kg^{-1} $NaHCO_3$ solution to which sufficient HCl was added to lower its pH to 6.4. This pH pulse had distinct effects on the dissolution rates measured from Si, Al, and Mg versus Ca concentrations. The dissolution rates calculated from Si, Al, and Mg release decreased following this pH pulse consistent with the decrease of basaltic glass dissolution rates over this pH range (c.f. Gislason and Oelkers, 2003), whereas dissolution rates from Ca release increased following this pH pulse consistent with the relatively rapid re-dissolution of a calcium carbonate phase. Note that the solubility of calcium carbonate phases increase dramatically with decreasing pH at these conditions (Plummer and Busenberg, 1982).

If all the non-stoichiometric Ca release is attributed to calcium carbonate precipitation, mass balance considerations indicate that 0.14 g of calcite precipitated during the first 42 days of experimental series 1. This mass of calcite, if homogeneously precipitated over the whole basaltic glass BET surface area, would have lead to a 1 μm thick secondary calcite layer on the ~8.9 g of glass present in the reactor. Nevertheless, Si release suggests that this precipitation has little effect on the glass dissolution rates. This observation suggests that the precipitated calcium carbonate is not passivating. This observation would be consistent with either the precipitation of the calcium carbonate independently from the glass surface or heterogeneously on this surface.

Experimental series 2 ran for 26 days as a replicate of series 1, but dissolution rates for this experiment suggest not only retention of Ca, but also of Si, Mg and Al in secondary mineral phases. Steady-state glass dissolution rates based on Si, Mg and Al are systematically 0.3 log units lower than the rates obtained in series 1. The steady-state dissolution rates based on Ca release of this series are identical to those observed in experimental series 1 consistent with calcite saturation. PHREEQC calculations indicate the reactive fluid was supersaturated with respect to calcite, dawsonite, gibbsite, clays and zeolites; SEM images coupled with EDX substantiated the precipitation of a secondary silica-rich phase as depicted in Fig. 1c. It was not possible, however, to identify this needle-shaped precipitate due to crystal size. The observed silicate needles do, however, exhibit the morphology of the zeolites mesolite and scolecite, which are supersaturated in the outlet solution. It seems likely that this precipitate is responsible for the lower Si and Al release rates observed in this experimental series relative to experimental series 1. EDX also detected carbon on the glass surface, but no carbonate crystals were visible. More sensitive surface analysis techniques might reveal the identity of the needles and the carbon phases on the glass surface. This is the only experiment where mineral phases other than calcium carbonate were observed. It is noteworthy that these secondary Si-rich precipitates do not form massive coatings on the glass surface. In contrast, passivating silica rims have been reported in

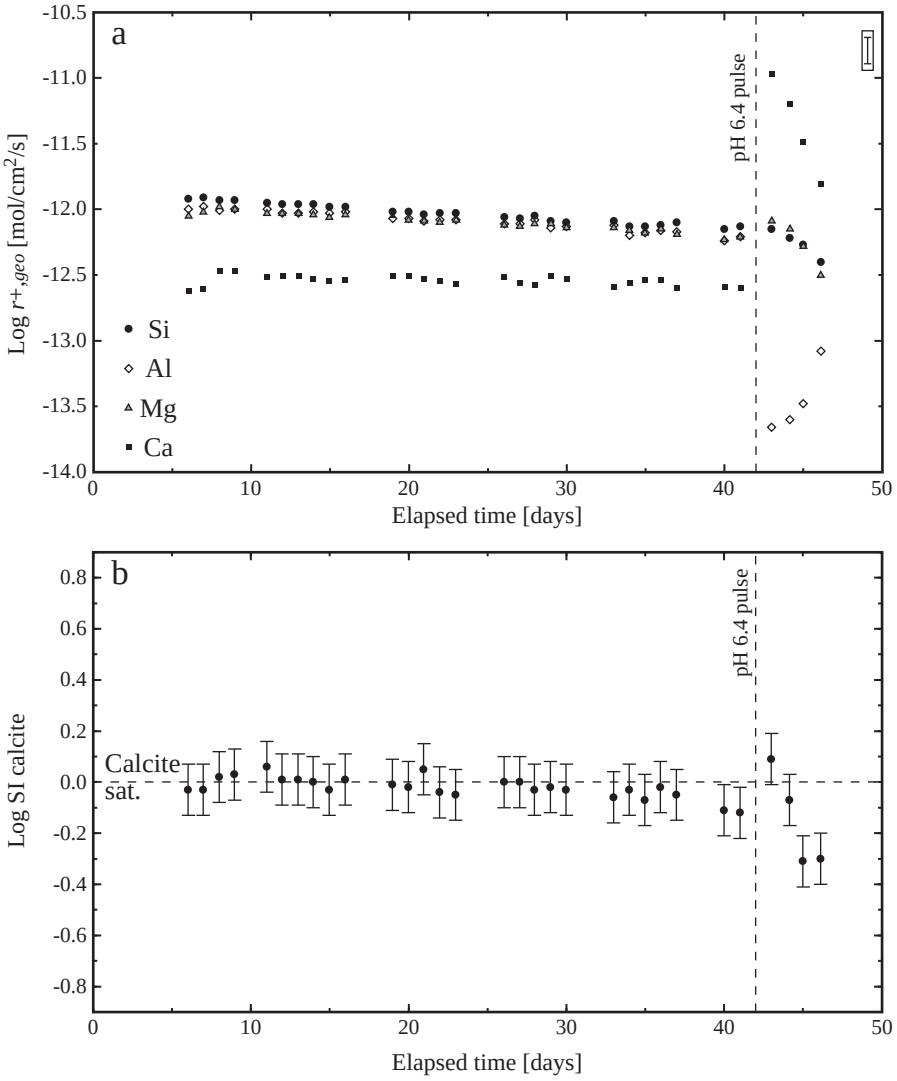

Fig. 3. a) Basaltic glass dissolution rates during experiment 1 at 70 °C and pH 8.2. A pH 6.4-pulse was added after 42 days of experiment. The uncertainty in the measured rates is ± 0.15 log units as illustrated by the error bar in the top-right corner of the plot. b) Calculated calcite saturation state of the reactive fluid during experiment 1. The error bars in this plot correspond to ± 0.10 uncertainty in log SI calcite values.

some previous studies (e.g. Béarat et al., 2006; Andreani et al., 2009; Daval et al., 2009b).

4.2. Basaltic glass dissolution in carbonate-rich fluids at 25 °C (experimental series 8 and 9)

Experimental series 8 consisted of the dissolution of basaltic glass in a solution containing 0.01 mol kg^{-1} $NaHCO_3$ and 0.01 mol kg^{-1} Na_2CO_3. The resulting inlet solution had a pH of 10.0. The results of experiment 8a are presented as a function of time in Fig. 4a. Dissolution rates from Si, Mg, and Ca release are similar and consistent with stoichiometric dissolution of the glass during the first 100 days duration of the experiment. After 100 days, Ca appears to be preferentially released from the glass. The reason for this preferential Ca release is unclear, but post-experimental SEM images (e.g., Fig. 1d) clearly indicate that calcium carbonate precipitated on the basaltic glass surface. This is also corroborated by calculations showing that the reactive fluid was saturated with calcite throughout the experiment. Dissolution rates calculated from Al release are relatively low suggesting precipitation of an Al-bearing phase. As was the case for experimental series 1, Si and Mg release appear nearly constant during the 140-day experiment.

A parallel control experiment, experimental series 9, was performed by dissolving basaltic glass in a pH 9.9 solution comprised of 0.035 mol kg^{-1} NaCl + 0.13 mmol kg^{-1} NaOH. Dissolution rates based on Si release from experiment 9a are compared to those of experiment 8a in Fig. 4b. It can be seen that dissolution rates from Si release from both experiments are identical within experimental uncertainty. SEM images of basaltic glass powders following experimental series 9 show the basalt surfaces to be free of secondary minerals (Fig. 1e).

4.3. Basaltic glass dissolution in calcium-bearing aqueous carbonate fluids at 25 °C (experimental series 4 and 6)

In an attempt to assess the effect of thicker calcium carbonate layers on basaltic glass dissolution, two further sets of basaltic glass dissolution experiments were carried out using calcium bearing aqueous carbonate inlet fluids at 25 °C (series 4 and 6). Two inlet solutions were connected to the mixed-flow reactor; one injecting an aqueous 0.035 mol kg^{-1} $NaHCO_3$ solution and the other aqueous solution containing 0.01 to 0.03 mol kg^{-1} $CaCl_2$ and sufficient NaOH to attain the target pH. The compositions of these inlet solutions are listed in Table 2.

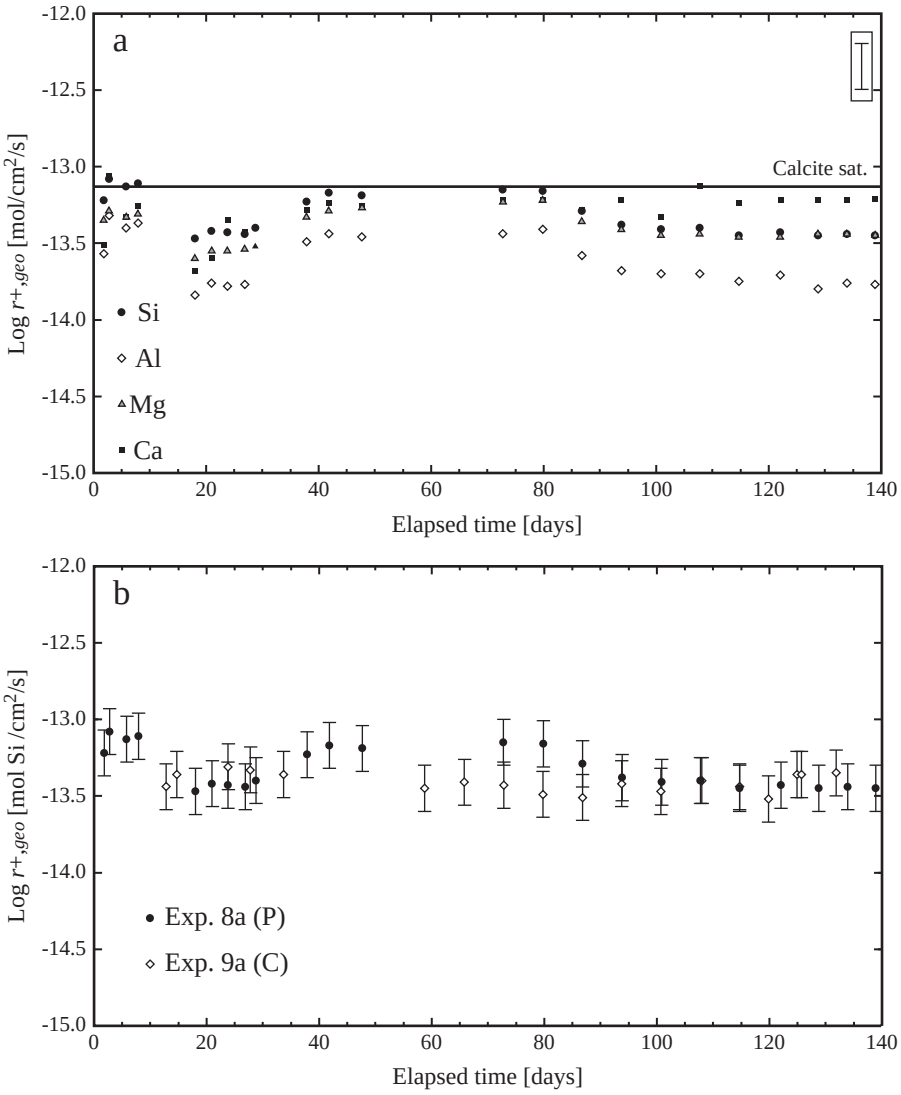

Fig. 4. a) Measured basaltic glass dissolution rates based on Si, Mg, Al, and Ca during experiment 8a (P) at 25 °C and pH 10.0. The error bars in this plot correspond to ± 0.15 log units uncertainty on the rates, and the solid line represents the Ca release rate needed to reach calcite saturation. b) Comparison of the dissolution rates based on Si release during experiment 8a (P) with the Si rates of the corresponding control experiment 9a (C) at 25 °C. 'P' and 'C' refers to precipitation and control experiments, respectively.

Basaltic glass dissolution rates based on Si during experimental series 4 and 6 are shown in Fig. 5, together with corresponding rates from control experiments (series 5 and 7, c.f. Table 3). Basaltic glass dissolution rates in precipitation and control experiments are identical within uncertainty and are invariant over time.

SEM images of both 'precipitation' and 'control' experiments are shown in Fig. 1f, g and h. No secondary minerals are evident in the 'control' experiments (series 5 and 7, Fig. 1h), and only calcium carbonate minerals (calcite and aragonite, based on morphology) are apparent in the 'precipitation' experiments (series 4 and 6, Fig. 1f and g). In contrast to the SEM images of the glass after experimental series 8, the calcium carbonate precipitates in series 4 and 6 did not grow on the basaltic glass surface but as individual crystals. This differing behavior may stem from two factors. First, the source of calcium in the fluids of experimental series 8 is the dissolution of the basaltic glass rather than the inlet fluid. Secondary, the inlet fluid in experimental series 4 and 6 are far more supersaturated with respect to calcite than the fluid in experimental series 8. This higher degree of supersaturation could provoke heterogeneous nucleation of calcium carbonate in the fluid of experimental series 4 and 6. Indeed, the weight of the solids after the experimental series 6 indicated that approximately 5 g of carbonates had precipitated inside the reactor; this estimate was qualitatively corroborated by Ca mass balance calculations that suggested that ~10 g of calcite precipitated during the 69-day duration of experiments 6a and 6b. Despite the fact that the mass of precipitated carbonates was substantial, glass dissolution rates were not affected. XRD analysis of post-experiment samples confirmed the presence of calcite in both experiments, whereas aragonite and vaterite, a third polymorph of $CaCO_3$, were not detected by XRD. However, the presence of aragonite in these experiments is very probable because the elongated crystals, seen in Fig. 1g are typical of orthorhombic aragonite (Palache et al., 1951). No cation impurities such as Mg or Sr, that could help distinguish between calcite and aragonite in the crystal structure, were detected with EDX (Gobac et al., 2009).

4.4. Comparison with previously published basaltic glass dissolution rates

The logarithm of steady state dissolution rates obtained in this study at 25 °C are plotted in Fig. 6 as a function of $\log\cdot(a_{H^+}^3 / a_{Al^{3+}})$ where a_i refers to the activity of the subscripted aqueous species. Only data for those outlet fluids where Si and Al release was stoichiometric

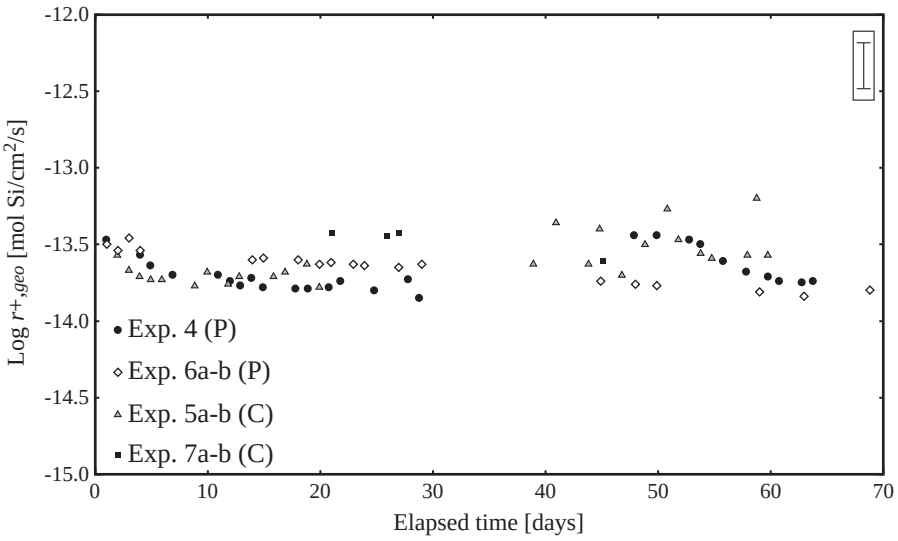

Fig. 5. Comparison of measured basaltic glass dissolution rates from Si release during experiments 4 and 6a–b with Si release during the corresponding control experiments 5a–b and 7a–b at 25 °C and pH ~ 7. The uncertainty on the rates is ±0.15 log units as illustrated by the error bar in the top-right corner. 'P' and 'C' refers to precipitation and control experiments, respectively.

are plotted in Fig. 6 to avoid potential ambiguities due to potential secondary mineral precipitation. Consistent with the dissolution mechanism and rate equations provided by Oelkers and Gislason (2001) and Gislason and Oelkers (2003) the far-from-equilibrium dissolution rates from the 'precipitation' as well as 'control' series can be expressed as

$$r_{Si,geo} = k\left(\frac{a_{H^+}^3}{a_{Al^{3+}}}\right)^n \quad (3)$$

where k denotes a rate constant and n a reaction order equal to 0.33. Eq. (3) is based on the assumption that the rate limiting step of basaltic glass dissolution is the breaking of partially liberated Si-tetrahedras through proton/aluminum exchange reactions (Oelkers, 2001; Wolff-Boenisch et al., 2004b; Schott et al., 2009). It can be seen in Fig. 6 that the dissolution rates of basaltic glass measured in the presence of precipitating $CaCO_3$ are similar to those measured in the 'control' experiments.

Several past studies reported dissolution rates of glasses similar to that used in this study at similar temperatures and pH. A compilation of these rates is given in Table 5. Rates normalized to BET surface area are comparable to those determined in this study, whereas rates normalized to geometric surface area are approximately one log unit lower than those obtained in this study.

A comparison of measured basaltic glass dissolution rates based on Si release as a function of fluid phase ionic strength is illustrated in Fig. 7. No effect of ionic strength is apparent.

5. Discussion

The results summarized above suggest that the presence of calcite precipitating on or near the surfaces of basaltic glass does not affect its dissolution rate. What calcium carbonate is observed to precipitate on these surfaces forms prisms rather than pervasive coatings covering

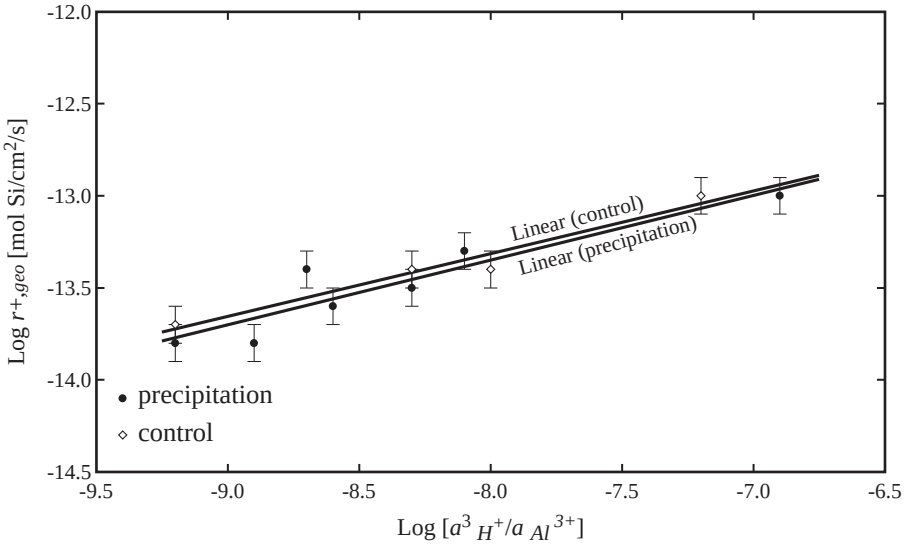

Fig. 6. Variation of measured basaltic glass dissolution rates, based on Si release, as a function of log $(a_{H^+}^3/a_{Al^{3+}})$ for all experiments at 25 °C for which stoichiometric Si/Al release was observed (see Table 3a). The uncertainty on the rates is ±0.15 log units as illustrated by the error bars. The linear equation for the control data is $\log r_{+,geo} = 0.34 \log (a_{H^+}^3/a_{Al^{3+}}) - 10.59$, $R^2 = 0.96$, and the corresponding equation for the precipitation data is $\log r_{+,geo} = 0.35 \log (a_{H^+}^3/a_{Al^{3+}}) - 10.53$, $R^2 = 0.86$.

Table 5
Steady-state Si dissolution rates (log r_+) in mol/cm^2/s at 25 °C reported in the literature.

pH	log $r_{+,BET}$ [a]	log $r_{+,BET}$ [b]	log $r_{+,geo}$ [b]	pH [c]	log $r_{+,BET}$ [c]	log $r_{+,geo}$ [c]
7.0	−15.1	−14.9	−12.9	7.0	−15.1	−13.7
8.0	−14.8	−14.6	−12.6	7.9	−14.7	−13.3
8.5		−14.4	−12.4	8.6	−14.8	−13.4
10.0	−14.1	−13.9	−11.9	10.1	−14.3	−13.0

[a] From Oelkers and Gislason (2001).
[b] From Gislason and Oelkers (2003), a roughness factor of 92 is used to calculate $r_{+,geo}$ from $r_{+,BET}$.
[c] This study, average of values given in Table 3b. The basaltic glass roughness factor is 23.

the whole original surface. These observations are consistent with those of Cubillas et al. (2005) who concluded that substantial inhibition of mineral dissolution by a precipitating phase is only efficient when there is a close crystal structural match between the dissolving and precipitating phase. As basaltic glass has a far different structure than precipitating calcium carbonate phases there is little thermodynamic drive to precipitate pervasive coatings on the surface of the primary mineral.

Another interesting observation is that the location of secondary precipitates apparently depends on the source of the material used to create the secondary phase and/or the degree of supersaturation of the fluid phase. In experiments where Ca was sourced from the dissolving basaltic glass (e.g. experimental series 8) precipitating calcite formed on the surfaces of the dissolving glass (see Fig. 1d). In contrast, in experiments where calcite was externally sourced and the fluids had higher degrees of supersaturation, calcite formed as distinct crystals separated from the glass surface (see Fig. 1f). This suggests that the location of secondary precipitates in natural systems may hold information on the source of its constituent elements. This conclusion is consistent with that of Putnis (2009) who reported that mineral replacement reactions are favored when the primary phase contributes elements to the secondary phase.

The observation that the presence of calcium carbonate precipitates does not inhibit basaltic glass dissolution favors the use of basalt for CO_2 carbonatization. This carbonatization process involves the release of Ca, Mg, and Fe from basalt by dissolution. These divalent metals can then react with dissolved CO_2 in the fluid phase to form stable carbonate minerals. It has been argued that basalt dissolution is the slowest and thus rate-limiting step of this coupled process. The observation that calcium carbonate precipitates do not create passivating layers on the basaltic glass surface suggests that Ca, Mg, and Fe release will not be slowed by carbonate precipitation at least at the initial part of the injection. The calcite growth may become more extensive with time, as was observed on basaltic grains by Schaef et al. (2009), though dissolution rates were not reported in this previous study.

6. Conclusions

The presence of calcite precipitate either on or adjacent to basaltic glass does not affect the dissolution rates of the primary phase. In fact the dissolution rates of basalt glass appear to be constant for at least 144 days despite the precipitation of substantial calcite during the experiments. This result favors long-term mineral sequestration in glassy volcanic rocks. In addition, the measured steady-state BET rates match those previously reported in the literature; supporting their application to describing chemical mass transfer rates in natural systems.

The observations presented above also confirm previous conclusions that non-pervasive secondary precipitates do not significantly influence the dissolution rates of the primary phase. This contrasts to the behavior of those systems where pervasive passivating surface precipitates form. In these latter systems rates can be slowed dramatically (c.f., Cubillas et al., 2005). It appears, therefore that the key to determining if a secondary precipitate will affect the dissolution rates of a primary phase is the understanding of the morphology and location of the secondary precipitates which is likely a function of 1) the relative structures of the primary and secondary phases, 2) the degree of supersaturation of the reactive fluid with respect to the secondary phase, and 3) the location of the source of the elements comprising the secondary phase. Further experiments attempting to illuminate the affect of calcium carbonate precipitation on the dissolution rates of other solids will be reported in future publications.

Acknowledgments

This study is part of the CarbFix project (www.carbfix.com) in Iceland, and we would like to thank all colleagues and co-workers within this project, in particular Helgi A. Alfredsson, Therese K. Flaathen, Snorri Guðbrandsson, Alex P. Gysi, Mahnaz Rezvani Khalilabad, Jürg

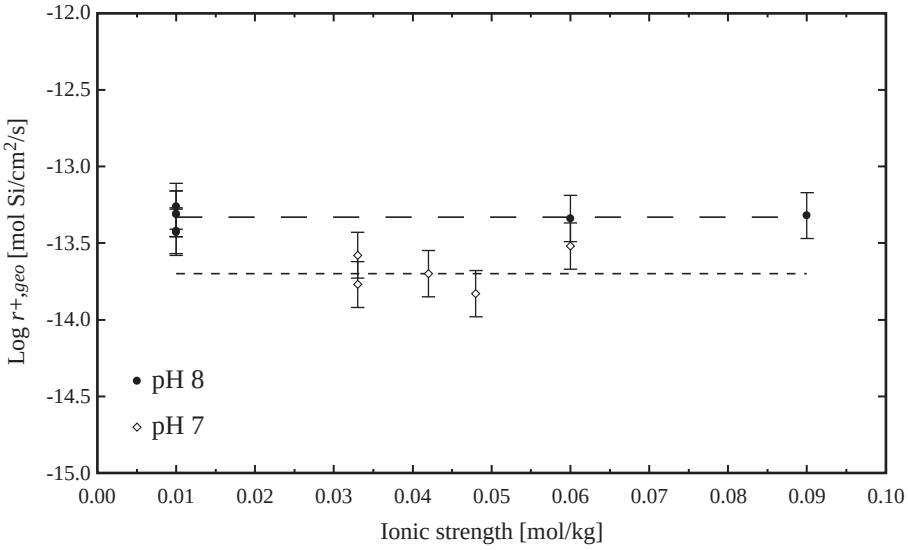

Fig. 7. Variation of measured steady-state basaltic glass Si dissolution rates as a function of ionic strength at 25 °C and pH 7 and 8. Rates were obtained from both 'precipitation' and 'control' experiments and the error bars on this plot correspond to ±0.15 log units uncertainty on the rates. The dashed lines are added to aid the reader.

Matter, Andri Stefánsson and Martin Stute. We thank the editor, Uwe Brand, and two anonymous reviewers, whose comments greatly improved this manuscript. We would also like to thank several colleagues for their help, in particular Eydís Salome Eiríksdóttir and Ingvi Gunnarsson at the University of Iceland, and Hólmfríður Sigurðardóttir at Reykjavík Energy. We are grateful for the SEM technical support provided by Jón Matthíasson at the Innovation Center Iceland and Sophie Gouy at LMTG-CNRS in Toulouse, France. We are also indebted to Caroline Piper Hem at the University of Copenhagen and Vasileios Mavromatis at LMTG-CNRS in Toulouse for assistance with XRD interpretations. We would also like to thank Erik Sturkell for graphical assistance and continued support. Reykjavík Energy, Nordurál and Hitaveita Suðurnesja and the European Community through the MIN-GRO Research and Training Network (MRTN-CT-2006-035488) are gratefully acknowledged for their financial support.

References

Alfredsson, H.A., Hadrarson, B.S., Franzson, H., Gislason, S.R., 2008. CO_2 sequestration in basaltic rock at the Hellisheidi site in SW Iceland: stratigraphy and chemical composition of the rocks at the injection site. Min. Mag. 72, 1–5.

Andreani, M., Liquot, L., Gouze, P., Godard, M., Hoise, E., Gibert, B., 2009. Experimental study of carbon sequestration reactions controlled by the percolation of CO_2-rich brine through peridotites. Eviron. Sci. Technol. 43, 1226–1231.

Béarat, H., McKelvey, M.J., Chizmeshya, A.V., Gormley, D., Nunez, R., Carpenter, R.W., Squires, K., Wolf, G.H., 2006. Carbon sequestration via aqueous olivine mineral carbonation: role of passivating layer formation. Eviron. Sci. Technol. 40, 4802–4808.

Benezeth, P., Palmer, D.A., Anovitz, L.M., Horita, J., 2007. Dawsonite synthesis and reevaluation of its thermodynamic properties from solubility measurements: implications for mineral trapping of CO_2. Geochim. Cosmochim. Acta 71, 4438–4455.

Cailleteau, C., Angeli, F., Devreux, F., Gin, S., Jestin, J., Jollivet, P., Spalla, O., 2008. Insight into silicate-glass corrosion mechanisms. Nat. Mat. 7, 978–983.

Chaïrat, C., Schott, J., Oelkers, E.H., Lartigue, J.-E., Harouiya, N., 2007. Kinetics and mechanism of natural fluorapatite dissolution at 25 °C and pH from 3 to 12. Geochim. Cosmochim. Acta 71, 5901–5912.

Cubillas, P., Köhler, S., Prieto, M., Causserand, C., Oelkers, E.H., 2005. How do mineral coatings affect dissolution rates? An experimental study of coupled $CaCO_3$ dissolution–$CdCO_3$ precipitation. Geochim. Cosmochim. Acta 69, 5459–5476.

Daval, D., Martinez, I., Corvisier, J., Findling, N., Goffe, B., Guyot, F., 2009a. Carbonation of Ca-bearing silicates, the case of wollastonite: experimental investigations and kinetic modeling. Chem. Geol. 265, 63–78.

Daval, D., Martinez, I., Guigner, J.-M., Hellmann, R., Corvisier, J., Findling, N., Dominici, C., Goffe, B., Guyot, F., 2009b. Mechanism of wollastonite carbonation deduced from micro- to nanometer length scale observations. Am. Mineral. 94, 1707–1726.

Gautelier, M., Oelkers, E.H., Schott, J., 2007. An experimental study of dolomite dissolution rates at 80 °C as a function of chemical affinity and solution composition. Chem. Geol. 242, 509–517.

Gautier, J.-M., Oelkers, E.H., Schott, J., 2001. Are quartz dissolution rates proportional to BET surface areas? Geochim. Cosmochim. Acta 65, 1059–1070.

Giammar, D.E., Bruant Jr., R.G., Peters, C.A., 2005. Forsterite dissolution and magnesite precipitation at conditions relevant for deep saline aquifer storage and sequestration of carbon dioxide. Chem. Geol. 217, 257–276.

Gislason, S.R., Oelkers, E.H., 2003. Mechanism, rates and consequences of basaltic glass dissolution: II. An experimental study of the dissolution rates of basaltic glass as a function of pH and temperature. Geochim. Cosmochim. Acta 67, 3817–3832.

Gislason, S.R., Wolff-Boenisch, D., Stefansson, A., Oelkers, E.H., Gunnlaugsson, E., Sigurdardóttir, H., Sigfússon, G., Brocker, W.S., Matter, J., Stute, M., Axelsson, G., Fridriksson, T., 2010. Mineral sequestration of carbon dioxide in basalt: a pre-injection overview of the CarbFix project. Int. J. Greenhouse Gas Control 4, 537–545.

Gobac, Ž.Ž., Posilović, H., Bermanec, V., 2009. Identification og biogenetic calcite and aragonite using SEM. Geol. Croat. 62 (3), 201–206.

Goldberg, D.S., Takahashi, T., Slagle, A.L., 2008. Carbon dioxide sequestration in deep-sea basalt. Proc. Natl Acad. Sci. 105, 9920–9925.

Gysi, A., Stefansson, A., submitted for publication. CO_2–water–basalt interaction II. Numerical simulation of low temperature CO_2 sequestration into basalts. Reaction modeling, *submitted to Geochim. Cosmochim. Acta*.

Helgeson, H.C., Murphy, W.M., Aagaard, P., 1984. Thermodynamic and kinetic constraints on reaction rates among minerals and aqueous solutions. II. Rate constants, effective surface area, and the hydrolysis of feldspars. Geochim. Cosmochim. Acta 48, 2405–2432.

Hodson, M.E., 2003. The influence of Fe-rich coatings on the dissolution of anorthite at pH 2.6. Geochim. Cosmochim. Acta 67, 3355–3363.

Lasaga, A.C., 1984. Chemical kinetics of water–rock interactions. J. Geophys. Res. 89 (B6), 4009–4025.

Lasaga, A.C., 1998. Kinetic Theory in the Earth Sciences. Princeton Series in GeochemistryPrinceton University Press, Princeton, New Jersey. 811 pp.

Lee, M.R., Brown, D.J., Hodson, M.E., MacKenzie, M., Smith, C.L., 2008. Weathering microenvironments on feldspar surfaces: implications for understanding fluid-mineral reactions in soils. Min. Mag. 71, 1319–1328.

Marini, L., 2007. Geological Sequestration of Carbon Dioxide. Thermodynamics, Kinetics and Reaction Path modeling. Elsevier, Amsterdam. 470 pp.

Matter, J.M., Takahashi, T., Goldberg, D., 2007. Experimental evaluation of in situ CO_2–water–rock reactions during CO_2 injection in basaltic rocks: implications for geological CO_2 sequestration. Geochem. Geophys. Geosyst. 8, Q02001. doi:10.1029/2006GC001427.

McGrail, B.P., Schaef, H.T., Ho, A.M., Chien, Yi-Ju, Dooley, J.J., Davidson, C.L., 2006. Potential for carbon dioxide sequestration in flood basalts. J. Geophys. Res. 111. doi:10.1029/2005JB004169 B12201.

Murakami, T., Kogure, T., Kadohara, H., Ohnuki, T., 1998. Formation of secondary minerals and its effect on anorthite dissolution. Am. Mineral. 83, 1209–1219.

Nugent, M.A., Brantley, S.L., Pantano, C.G., Maurice, P.A., 1998. The influence of natural mineral coatings on feldspar weathering. Nature 395, 588–591.

Oelkers, E.H., 2001. General kinetic description of multioxide silicate mineral and glass dissolution. Geochim. Cosmochim. Acta 65, 3703–3719.

Oelkers, E.H., Cole, D.R., 2008. Carbon dioxide sequestration: a solution to a global problem. Elements 4, 305–310.

Oelkers, E.H., Gislason, S.R., 2001. The mechansim, rates and consequences of basaltic glass dissolution: I. An experimental study of the dissolution rates of basaltic glass as a function of aqueous Al, Si and oxalic acid concentration at 25 °C and pH = 3 and 11. Geochim. Cosmochim. Acta 65, 3671–3681.

Oelkers, E.H., Schott, J., 2005. Geochemical aspects of CO_2 sequestration. Chem. Geol. 217, 183–186.

Oelkers, E.H., Gislason, S.R., Matter, J., 2008. Mineral carbonation of CO_2. Elements 4, 333–337.

Pačes, T., 1983. Rate constants of dissolution derived from the measurements of mass balance in hydrological catchments. Geochim. Cosmochim. Acta 47, 1855–1863.

Palache, C., Berman, H., Frondel, C., 1951. The system of mineralogy of James Dwight Dana and Edward Salisbury Dana, 7th Edition. Halides, Nitrates, Borates, Carbonates, Sulfates, Phosphates, Arsenates, Tungstates, Molibdates, etc., Vol. 2. John Wiley and Sons, New York. 1124 pp.

Park, A.-H.A., Fan, L.-S., 2004. CO_2 mineral sequestration: physically activated dissolution of serpentine and pH swing process. Chem. Eng. Sci. 59, 5241–5247.

Parkhurst, D.L., Appelo, C.A.J., 1999. User's Guide to PHREEQC (version 2) — A Computer Program for Speciation, Batch-reaction, One-dimensional Transport, and Inverse Geochemical Calculations. USGS-Report 99-4259.

Plummer, L.N., Busenberg, E., 1982. The solubilities of calcite, aragonite and vaterite in CO_2–H_2O solutions between 0 and 90 °C, and an evaluation of the aqueous model for the system $CaCO_3$–CO_2–H_2O. Geochim. Cosmochim. Acta 46, 1011–1040.

Pokrovsky, O.S., Schott, J., Castillo, A., 2005. Kinetics of brucite dissolution at 25 C in the presence of organic and inorganic ligands and divalent metals. Geochim. Cosmochim. Acta 69, 905–918.

Putnis, A., 2009. Mineral replacement reactions. Rev. Mineral. Geochem. 70, 87–124.

Schaef, H.T., McGrail, B.P., 2009. Dissolution of Columbia River Basalt under mildly acidic conditions as a function of temperature: experimental results relevant to the geological sequestration of carbon dioxide. Appl. Geochem. 24, 980–987.

Schaef, H.T., McGrail, B.P., Owen, A.T., 2009. Basalt–CO_2–H_2O interactions and variability in carbonate mineralization rates. Energy Procedia 1, 4899–4906.

Schaef, H.T., McGrail, B.P., Owen, A.T., 2010. Carbonate mineralization of volcanic province basalts. Int. J. Greenhouse Gas Control 4, 249–261.

Schott, J., Pokrovsky, O.S., Oelkers, E.H., 2009. The link between mineral dissolution/precipitation kinetics and solution chemistry. Rev. Mineral. Geochem. 70, 207–258.

Siegel, D.I., Pfannkuch, H.O., 1984. Silicate dissolution influence on Filson Creek chemistry, northeastern Minnesota. Geol. Soc. Am. Bull. 95, 1446–1453.

Stockmann, G.J., Wolff-Boenisch, D., Gíslason, S.R., Oelkers, E.H., 2008. Dissolution of diopside and basaltic glass: the effect of carbonate coating. Min. Mag. 72, 139–143.

Velbel, M.A., 1993. Formation of protectiye surface layers during silicate-mineral weathering under well-leached oxidizing conditions. Am. Mineral. 78, 405–414.

Verney-Carron, A., Gin, S., Frugier, P., Libourel, G., 2010. Long-term modelling of alteration-transport coupling: application to a fractured Roman glass. Geochim. Cosmochim. Acta 74, 2291–2315.

White, A.F., Brantley, S.L., 2003. The effect of time on the weathering of silicate minerals: why do weathering rates differ in the laboratory and field? Chem. Geol. 202, 479–506.

Wolff-Boenisch, D., Gislason, S.R., Oelkers, E.H., Putnis, C.V., 2004a. The dissolution rates of natural glasses as a function of their composition at pH 4 and 10.6, and temperatures from 25 to 74 °C. Geochim. Cosmochim. Acta 68, 4843–4858.

Wolff-Boenisch, D., Gislason, S.R., Oelkers, E.H., 2004b. The effect of fluoride on the dissolution rates of natural glasses at pH 4 and 25 °C. Geochim. Cosmochim. Acta 68, 4571–4582.

Wolff-Boenisch, D., Gislason, S.R., Oelkers, E.H., 2006. The effect of crystallinity on dissolution rates and CO_2 consumption capacity of silicates. Geochim. Cosmochim. Acta 70, 858–870.

Zhu, C., 2005. In situ feldspar dissolution rates in an aquifer. Geochim. Cosmochim. Acta 69, 1435–1453.

Zhu, C., Veblen, D.R., Blum, A.E., Chipera, S.L., 2006. Naturally weathered feldspar surfaces in the Navajo sandstone aquifer, Black Mesa Arizona: electron microscopic characterization. Geochim. Cosmochim. Acta 70, 4600–4616.

Zhu, C., Lu, P., Zheng, Z., Ganor, J., 2010. Coupled alkali feldspar dissolution and secondary mineral precipitation in batch systems: 4. Numerical modeling of kinetic reaction paths. Geochim. Cosmochim. Acta 74, 3963–3983.